CHAPTER II

LITERATURE REVIEW

2.1 Introduction

This chapter provides a comprehensive review of foundational studies related to the finite element method (FEM), including simplified models frequently employed in drop impact analysis, material characterization, and nonlinear cushion modeling. In addition, various computational approaches utilized in the simulation of foam net cushioning systems are discussed.

2.2 Transportation damage

Mechanical damage is a critical factor influencing the postharvest quality of fruits during transportation. External forces such as impacts and vibrations are primary contributors to this form of deterioration. Specifically for guava, quality degradation during transit not only results in substantial economic losses but also exacerbates postharvest fruit waste.

Bruising refers to a form of latent mechanical injury that is not immediately visible upon occurrence (Mei et al. 2023). Such damage commonly arises during transportation, sorting, and packaging operations, and contributes significantly to the deterioration of kiwifruit. Due to its high susceptibility to mechanical stress, particularly from external impacts, kiwifruit is especially prone to this type of damage.

The primary cause of bruise damage during fruit handling is the application of excessive impact forces resulting from dropping onto packaging surfaces (Lin et al. 2023).

Similarly, reported that apples dropped onto rigid surfaces such as concrete or wood exhibited the most severe bruising (Stopa et al. 2018)., whereas foam surfaces

resulted in the least damage among four tested packaging materials during free-drop trials. Moreover, wooden packaging was found to provide inferior protection against mechanical injury when compared with telescopic fiberboard trays and plastic containers (Batt et al. 2019).Nonetheless, the extent of bruise damage in kiwifruit caused by impact with different packaging materials such as wood, high-density polyethylene (HDPE), and expanded polystyrene (EPS) remains inadequately understood.

2.3 Impact damage

Impact damage occurs when an object collides with a surface with sufficient force to rupture or separate cellular structures. The external manifestations typically include bruising or cracking. Common impact damage scenarios primarily arise from two mechanisms: the free fall of fruits from trees to the ground during harvesting operations, and dynamic impacts occurring between individual fruits or between fruits and packaging materials or containers. The latter damage mechanism results from various vibrational sources, including transportation vehicle vibrations, fruit containers subjected to transport-induced oscillations, and vibrations from conveyor belts in grading systems. Impact damage represents the most severe mechanical damage mechanism in fruit handling processes, significantly affecting post-harvest quality and economic value (Van Zeebroeck et al. 2007).

2.4 Impact damage to fresh produce

The two most common procedures for impact testing are: mounting the fruit with a pendulum impactor or dropping the fruit from a predetermined height onto an impact surface. In the drop test method, the impact energy (E_{impact}) is calculated using the equation $E = mgh$ where m is the mass of the sample (kg), g is the acceleration due to gravity (9.81 m/s²), and h is the drop height (m).

2.4.1. Package cushioning

One of the fundamental objectives of packaging engineering is to ensure that a product is transported from the point of manufacture to the point of sale without sustaining unacceptable levels of damage or loss (Yam. 2010). Packaging particularly through the use of cushioning materials plays a vital role in mitigating in-transit damage. However, packaging solutions must not only be effective but also economically and practically feasible.(Al-Dairi et al. 2022).

Most products require protective packaging because they are typically engineered to endure only their intended usage conditions, rather than the rigorous and unpredictable stresses encountered during distribution (Goodwin et al. 2011). Among the various hazards present in the distribution environment, the most prevalent include impacts, punctures, and deformation from manual handling; vibrations induced by vehicle motion; compression resulting from stacking; atmospheric changes at high altitudes; and fluctuations in relative humidity and temperature (Hatton. 1998).

2.4.2. Packaging as a green solution.

In general, foam net cushion packaging used for fresh produce particularly vegetables and fruits is predominantly designed for single-use applications. These cushions are typically manufactured from synthetic, non-biodegradable polymers, which contribute significantly to post-consumer environmental waste. Concurrently, plastic waste pollution has emerged as one of the most critical global environmental concerns.

Within this context, biodegradable plastics represent both considerable challenges and compelling opportunities. These include the need to enhance material performance, ensure cost-effectiveness, and develop scalable manufacturing processes. At the same time, such materials offer the potential to substantially mitigate the long-term environmental impacts associated with conventional plastic waste.

2.5 Finite element method

Principles finite element method The FEM process begins with discretizing the domain of the problem into smaller, simpler parts called elements. These elements are then analyzed using numerical techniques (Figure 2.1), often derived from partial differential equations, to obtain an approximate solution across the entire domain.

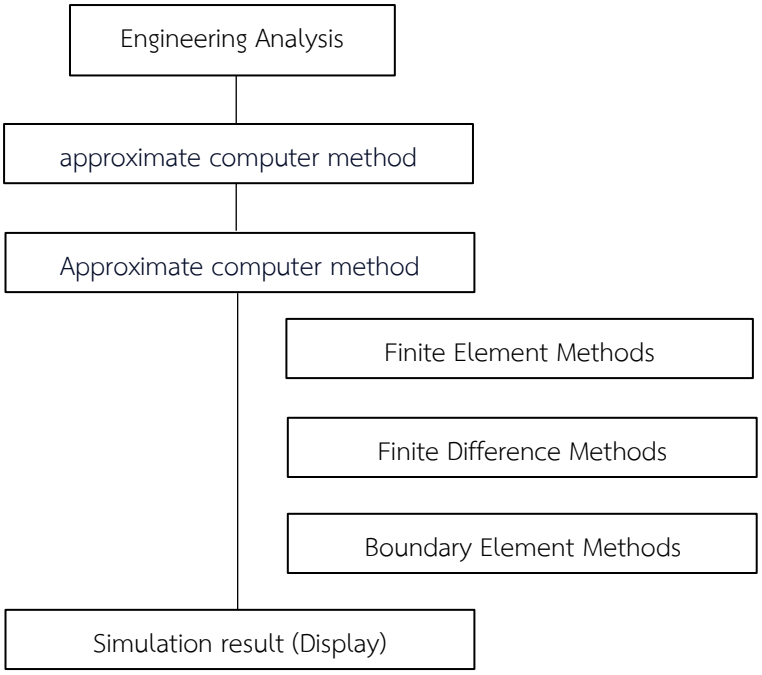

Figure 2.1 The process of computer aid designs and numerical techniques

The Finite Element Method (FEM), also known as Finite Element Analysis (FEA), is a computational technique used to obtain approximate solutions to boundary value problems in engineering. FEM is a numerical method that provides approximate solutions for a wide range of complex engineering problems. It has become an essential tool in modern engineering as shown in (Figure 2.2), extensively applied in the analysis, simulation, and design of real-world systems.

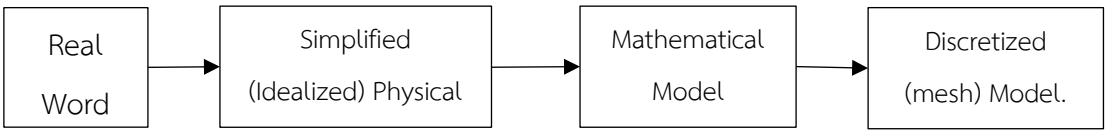

Figure 2.2 Workflow of pre-processing FEM simulation

2.5.1. Differential equation

Differential equation is partial differential (PDE), ordinary differential equation (ODE) is a equation that involves two or more unknown functions. Such equations aid in the relationship of function with several variables to their partial derivatives.

General Form of first-order partial derivatives equation.

A first-order partial derivative equation with *n* independent variables has general form.

$$F\ (x1, x2, \dots, xn, w, \frac{\partial w}{\partial x1}, \frac{\partial w}{\partial x2}, \dots, \frac{\partial w}{\partial x2}) = 0, \quad (1)$$

Where: $w{=}w\ (x1, x2, \dots, xn)$ is the unknow function

$F\ (\dots)$ is a given function.

Order of partial differential equations

$$\frac{\partial z}{\partial x} + \frac{\partial z}{\partial y} = x + zy \quad (2)$$

As the order of the highest derivative is 1.

Degree of partial differential equations

$$\frac{\partial z}{\partial x} + \frac{\partial z}{\partial y} = z + xy \quad (3)$$

Has 1 as the highest derivative is of the first degree.

2.6 FEM for solid mechanics problems

Equilibrium of rigid body and elastic behavior of solids

Triaxial stress represents a stress state wherein a stress element is subjected to three mutually perpendicular normal stresses, show in (Figure 2.3). The absence of shear stresses on the x, y, and z planes indicates that these three normal stresses constitute

the principal stresses of the system. This configuration is fundamental to the analysis of material behavior under complex loading conditions.(Gere et al. 1997).

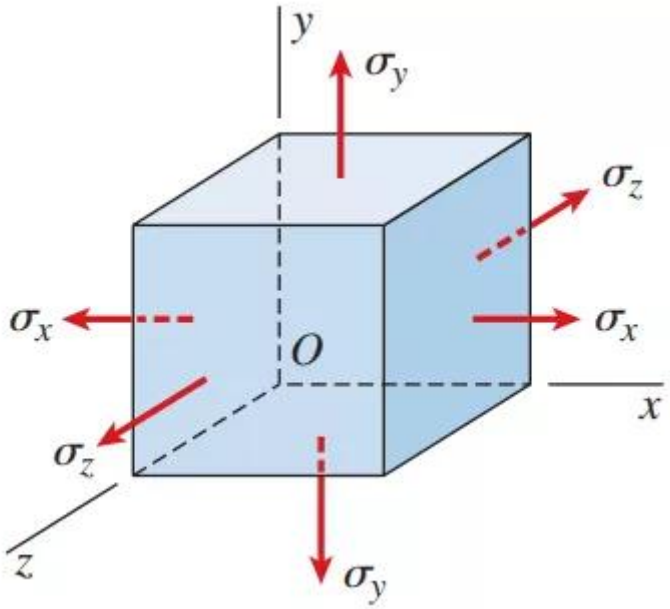

Figure 2.3 Triaxial Stress State (James Gere, 2008.)

Rigid objects in static equilibrium equation

$$\frac{\partial \sigma_x}{\partial x} + \frac{\partial \tau_{xy}}{\partial y} + \frac{\partial \tau_{xz}}{\partial z} + F_x = 0 \quad (4)$$

$$\frac{\partial \tau_{xy}}{\partial x} + \frac{\partial \sigma_x}{\partial y} + \frac{\partial \tau_{yz}}{\partial z} + F_y = 0 \quad (5)$$

$$\frac{\partial \tau_{xz}}{\partial x} + \frac{\partial \tau_{yz}}{\partial y} + \frac{\partial \sigma_z}{\partial z} + F_z = 0 \quad (6)$$

Where: $\sigma_x, \sigma_y, \sigma_z$ is axial or longitudinal stress x, y, z.

$\tau_{xy}, \tau_{xz}, \tau_{yz}$ is shear stress in axial x, y, z.

F_x, F_y, F_z is body force in axial x, y, z.

2.6.1. Surface traction

Boundary conditions may consist of many systems. One of the conditions is surface traction in general.

2.6.1.1 Traction (Stress) Vector

The traction vector (T) is defined as the ratio of the force vector acting upon a specified cross-section to the area of that cross-section. This fundamental parameter characterizes the distributed force intensity across the material interface and serves as a critical measure in continuum mechanics analyses

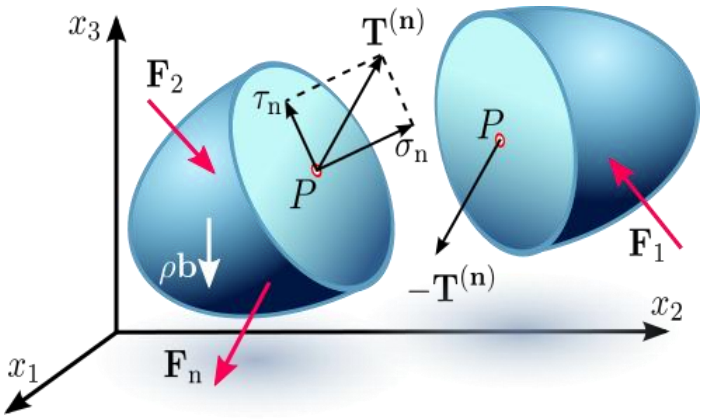

Figure 2.4 The traction vector (T), (stress vector at the point) on the surface surrounding the point with normal vector n is defined as.

Figure 2.4 depicts the stress vector T acting on an internal surface within a continuum, illustrating both normal and shear stress components on this surface. Additionally, the figure demonstrates the reaction stress vector -T operating on the opposing side of the internal surface, in accordance with Newton's Third Law of Motion, which stipulates the equivalence of action and reaction forces. This representation elucidates the fundamental stress transmission mechanism across internal material boundaries and the inherent equilibrium properties of continuous media under mechanical loading conditions (Truesdell. 1976).

$$T_n = \lim_{\Delta A \to 0} \frac{\Delta F}{\Delta A} \tag{7}$$

from Newton's laws of motion: $T_n = -t_{-n}$

$$\mathrm{T} = \frac{F_{internal}}{Area} \tag{8}$$

Stress Tensors and Traction Vectors.

$$\vec{T} = T_x\hat{\imath} + T_y j + T_z\hat{k} \tag{9}$$

Where: T_x, T_y, T_z is stress at surface in axial x, y, z respectively

$$\begin{Bmatrix} T_x \\ T_y \\ T_z \end{Bmatrix} = \begin{Bmatrix} \sigma_x & \tau_{xy}, & \tau_{xz} \\ \tau_{xy}, & \sigma_y & \tau_{yz} \\ \tau_{xz}, & \tau_{yz}, & \sigma_z \end{Bmatrix} \begin{Bmatrix} n_x \\ n_y \\ n_z \end{Bmatrix} \tag{10}$$

Where: n_x, n_y, n_z is vector cosine direction

$$n = n_x\hat{\imath} + n_y j + n_z\hat{k} \tag{11}$$

Boundenly condition vector vertical of surface the rigid body possible body possible show pre-strain shows the relationship between normal strain and normal stress. As shown in Figure 2.5

$$\{\sigma\} = [c]\{\varepsilon - \varepsilon_0\} \tag{12}$$

For

$$\{\sigma\}^T = \begin{bmatrix} \sigma_x & \sigma_y & \sigma_z & \tau_{xy} & \tau_{yz} & \tau_{xz} \end{bmatrix} \tag{13}$$

$$\{\varepsilon\}^T = [\varepsilon_x \ \ \varepsilon_y \ \ \varepsilon_z \ \ \gamma_{xy} \ \gamma_{yz} \ \gamma_{xz}] \tag{14}$$

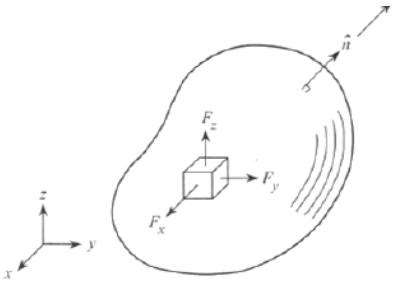

Figure 2.5 Rigid body equilibrium 3D

$$[\boldsymbol{C}] = \frac{E}{(1+\upsilon)(1-2\upsilon)}\begin{bmatrix} 1-\upsilon & \upsilon & \upsilon & 0 & 0 & 0 \\ \upsilon & 1-\upsilon & \upsilon & 0 & 0 & 0 \\ \upsilon & \upsilon & 1-\upsilon & 0 & 0 & 0 \\ 0 & 0 & 0 & \frac{(1-2\upsilon)}{2} & 0 & 0 \\ 0 & 0 & 0 & 0 & \frac{(1-2\upsilon)}{2} & 0 \\ 0 & 0 & 0 & 0 & 0 & \frac{(1-2\upsilon)}{2} \end{bmatrix} \quad (15)$$

Where: $\boldsymbol{\upsilon}$ is Poisson's ratio

Matrix $[\boldsymbol{C}]$ show the relationship between stress and strain and $\{\varepsilon_0\}$ are pre strain. And

$$\{\varepsilon_0\}^T = [\Delta T\ \Delta T\ \Delta T\ 0\ 0\ 0] \quad (16)$$

2.6.2. Three-dimensional isoperimetric elements.

Calculation of strains and stresses

Strains inside an element are determined with the use of the displacement differentiation matrix.

$$\{\varepsilon\} = [B] \quad (17)$$

Stresses are calculated with the Hook's law.

$$\{\varepsilon\} = [E]\{e\} = [E](\{\varepsilon\} - \{\varepsilon_0\}^T) \quad (18)$$

Where $\{\varepsilon_0\}^T$ is the vector of free thermal expansion.

2.7 Mesh generation

The successful of the finite element method simulation is the mesh generation show in Figure 2.6 (Sadrehaghighi. 2021)., In general hexahedral element was general element as it shows great accuracy and flexibility, in engineering problem CAD simulation very complex geometries hexahedral element impossible to generating, the complex

geometries trihedral element was flexibility and great the generating process show in Figure 2.7

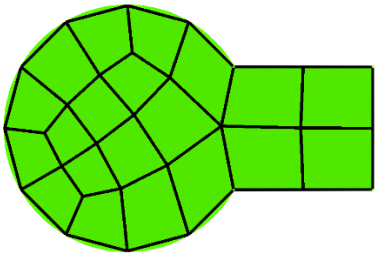

Figure 2.6 Finite element mesh of quadrilaterals of a curved domain.

Mesh generation process

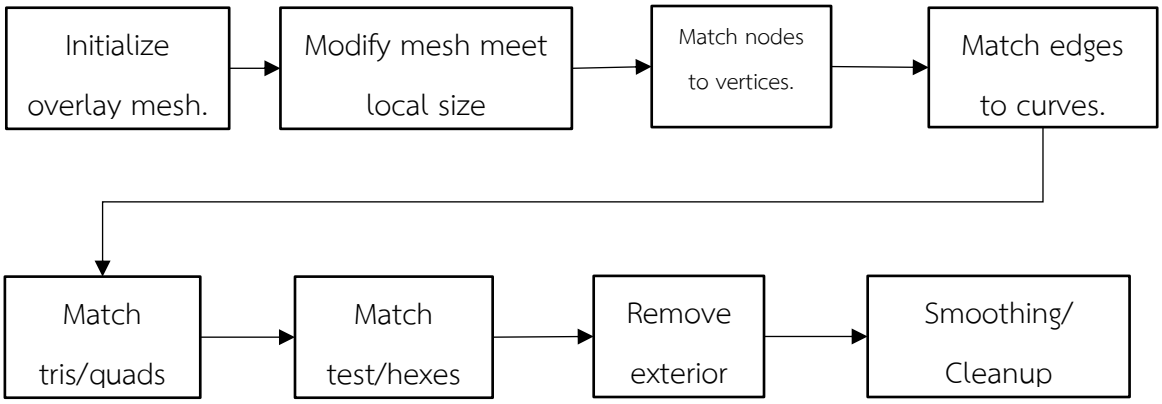

Figure 2.7 Mesh generation

2.8 Failure theories of material

The finite element method analysis to solve an engineering problem is defined by testing method by Yield Strength (**σ**y) or Ultimate Strength (**σ**u) are Failure analysis. The Failure analysis of martial consists of two types: Ductile Materia and Brittle Material, stress-strain curves as shown in Figure 2.8

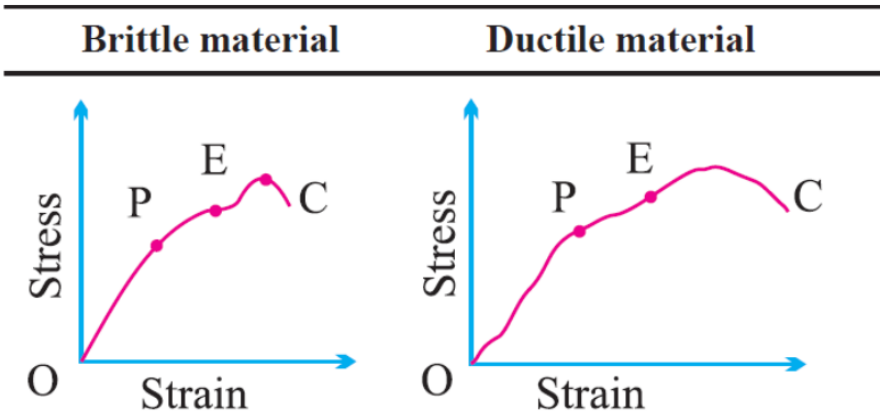

Figure 2.8 Stress-strain curves of brittle material, ductile material-compression test

2.8.1. Brittle fracture

For a brittle material, brittle facture takes place without any appreciable deformation, and by rapid crack propagation. The direction of crack motion is very nearly perpendicular to the applied tensile stress and yields a relatively fractured surface.

2.8.2. Ductile fracture

When ductile material has a gradually increasing tensile stress, it behaves elastically up to a limiting stress and then plastic deformation occurs. As stress is increased, the cross-sectional area of the material is reduced, and a necked region is produced.

A comprehensive universal theory of failure that encompasses all material properties and stress states remains elusive in continuum mechanics. Rather, the field has evolved through multiple hypotheses formulated and experimentally validated over several decades, as show in Figure 2.9. This evolutionary process has culminated in a collection of contemporary methodologies widely adopted by engineering practitioners. These methodologies, while not universally applicable across all material systems, provide pragmatic frameworks that guide modern design practices and failure prediction protocols in various engineering disciplines.

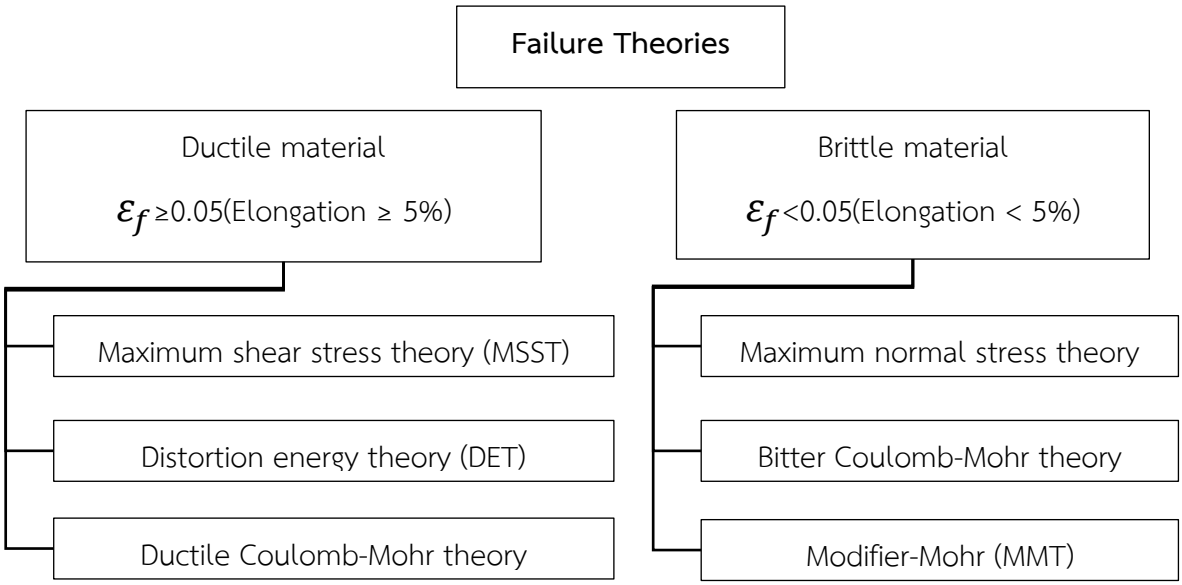

Figure 2.9 Diagram failure theories of material

Historical development of failure theories showing the relationship between theoretical models and their experimental validation. The convergence towards contemporary design methodologies is highlighted, demonstrating the progressive refinement of failure prediction capabilities over time.

2.8.3. Triaxial stress

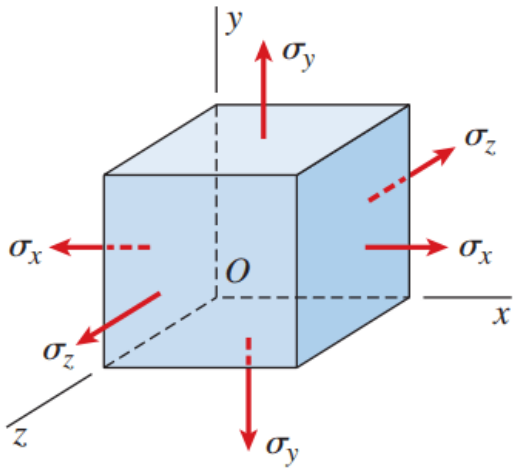

Figure 2.10 Triaxial stress state mechanics of materials (James Gere, 2008)

Triaxial stress is the stress state when a stress element is acted upon by three mutually normal stresses on the x, y, and z planes so the three normal stresses are the principal stresses.

Yield Strength (**σ**y) ductile materials

Ultimate Strength (**σ**u) brittle materials

Failure theories are defined as a function of the principal stress and the materials.

$$\boldsymbol{f}(\sigma_1, \sigma_2, \sigma_3) = \sigma_x, \sigma_y \tag{19}$$

Probably the simplest failure theory is to the failure occurred when the maximum or minimum principal stress as reach the yield or ultimate strengths of the material.

Rankine (maximum principal stress)

$$\sigma_1 = \sigma_y, \sigma_u \tag{20}$$

$$\sigma_3 = -\sigma_y, -\sigma_u \tag{21}$$

Maximum principal stress theory or Rankin theory

Failure of ductile materials

Hydrostatic stress does not cause yielding in ductile materials.

A general triaxial stress state like the one show decomposed into stresses which cause a change in volume and stress which cause shape distortion. Maximum Shear Stress

Elastic material show failure when Maximum Shear Stress higher than uniaxial stress tests show in Figure 2.11

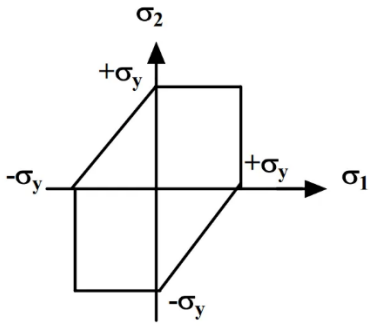

Figure 2.11 failure envelope as per maximum shear stress theory

$$\sigma_{eff} = \tau_{max} = \frac{\sigma_1 - \sigma_3}{2} \geq \frac{S_y}{2} \quad (22)$$

Where: $\sigma_A \geq \sigma_B \geq \sigma_C$ and $\sigma_A \geq \sigma_B$

1.) $\sigma_A \geq \sigma_B \geq 0$ by $\sigma_1 \geq \sigma_A$ and $\sigma_3 = 0$, $\sigma_A \geq S_y$

2.) $\sigma_A \geq 0 \geq \sigma_B$ by $\sigma_1 \geq \sigma_A$ and $\sigma_3 = 0$, $\sigma_A - \sigma_B \geq S_y$

3.) $0 \geq \sigma_A \geq \sigma_B$ by $\sigma_1 \geq \sigma_A$ and $\sigma_3 = \sigma_B \geq S_y$

Maximum Shear Stress theory creep failure

2.8.4. Von-Mises yield criteria.

The von Mises stress criterion serves as a principal methodology for predicting yield initiation in isotropic, ductile metallic materials subjected to complex loading conditions (Figure 2.12). This approach involves calculating the scalar von Mises stress value and comparing it with the material's yield stress, thereby implementing the von Mises Yield Criterion. The fundamental objective of this criterion is to establish a universally applicable yield prediction framework for ductile metals under arbitrary three-dimensional stress states, irrespective of the specific combination of normal and shear stresses present in the system. The von Mises stress effectively distills a complex triaxial stress state into a single scalar parameter that can be directly compared to the material's yield strength—a scalar value typically determined through uniaxial tensile testing, which represents the most straightforward experimental methodology for material characterization.

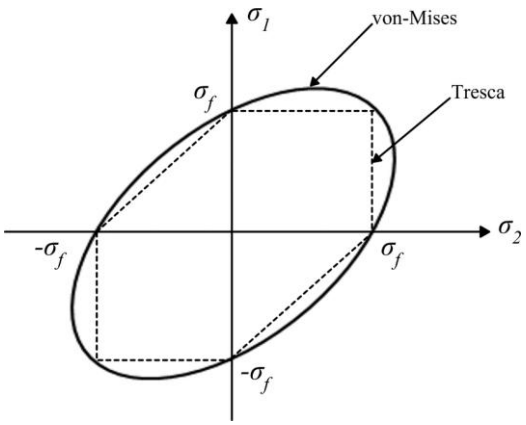

Figure 2.12 Comparison of the yield locus for the plane stress of von Mises yield criterion and Tresca yield criterion.

Figure 2.12 Three-dimensional representation of the von Mises yield surface in principal stress space. The cylindrical yield surface demonstrates the independence of yielding from hydrostatic stress components. The circular cross-section perpendicular to the hydrostatic axis ($\boldsymbol{\sigma_1 = \sigma_2 = \sigma_3}$) distinguishes the von Mises criterion from other yield criteria such as Tresca (hexagonal).